

Hyperspectral and Infrared Image Collaborative Classification Based on Morphology Feature Extraction

Dandan Cao, Mengmeng Zhang , Wei Li , *Senior Member, IEEE*, and Qiong Ran, *Senior Member, IEEE*

Abstract—With the development of sensor technology, fusion of multiple remote sensors has aroused wide attention in the earth observation area. In this article, we propose to integrate the complementary information of hyperspectral image (HSI) and infrared image (IFI) based on mathematical morphological methods. HSI contains rich spectral information and spatial information, but the operation methods using only hyperspectral data are still subject to many restrictions. IFI can capture infrared rays radiated in the object, but it has no advantage in dealing with complex terrain classification. HSI and IFI can acquire different information of objects, and the information between these two kinds of data has great complementarity. In order to make full use of the information provided by HSI and IFI, this article proposes an HSI and IFI collaborative classification framework based on a Threshold-based Local Contain Profile (TLCP), where TLCP is our new design for suppressing interferences within spatial extractions. Specifically, the spatial information of HSI and IFI is extracted by TLCP, and then, these features are integrated and fed into the support vector machine for object classification. Experimentally, we compare the proposed method with the existing LCP and EP and evaluate the collaborative framework using GF5 satellite data collected over Hebei Province in China. Final results demonstrated the effectiveness of the proposed method.

Index Terms—Extinction profile (EP), hyperspectral images (HSIs), infrared image (IFI), object classification, Threshold-Based Local Contain Profile (TLCP).

I. INTRODUCTION

WITH the development of remote sensing (RS) technology, a large amount of data is available, thus making remarkable progress in various applications [1]. The classification and identification of materials located above or below the surface of the earth has always been a challenging research topic in earth sciences and RS [2], [3]. In [4], for a high-spatial-resolution

RS image scene classification, a convolutional neural network based on the attention mechanism is proposed, which can capture class-specific features and eliminate redundant information, and promote the model to capture discriminative regions as much as possible. In [5], the application of hyperspectral image (HSI) in the classification of coast beaches, the artificial target recognition, mine detection, oil spill identification is introduced. In [6], multiscale superpixel segmentation and subspace-based support vector machine (SVM) are fused together to integrate spatial information for the HSI classification, and it shows effectiveness and reliability in the earth observation task. In [7], a novel dual-attention noise reduction network is proposed, which fully considers the global dependence and correlation between the spatial and spectral information of HSI, and applies it to HSI denoising. In [8], a domain adaptive strategy is proposed to adjust the semantic segmentation network through adversarial learning, which solves the problem of fine-grained mapping of urban villages (UVs) from satellite images, and adaptively obtaining similar outputs for input images from different domains. This strategy can significantly improve the pixel-level mapping of UVs.

HSI [9], [10] is a kind of RS image with rich spectral information. However, there is some redundant information within hyperspectral data, limiting the effectiveness of the single-HSI-source analysis. Recently, more and more research works have focused on a collaborative analysis of HSI with images from other sensors to improve classification performance. For example, although HSI has rich spectral information, it cannot distinguish objects with similar spectral features but different elevation. However, Light Detection And Ranging (LiDAR) data can obtain related elevation information. In [11], a feature-fusion-based method was proposed for HSI and LiDAR data classification, and this algorithm has achieved satisfying classification performance on the MUUFL Gulfport dataset. In [12], the joint classification of HSI and LiDAR data is studied by using a hierarchical random walk network. In [13], by combining the scattering information polarimetric synthetic aperture radar and spectral information of hyperspectral data, the classification accuracy of land use is improved. In [14], an object-based hyperspectral and LiDAR data fusion method is proposed, and multiscale information was integrated in cross-source utilization process, leading to an improved classification result on urban scene.

Manuscript received May 31, 2020; revised February 11, 2021; accepted April 1, 2021. Date of publication April 13, 2021; date of current version May 7, 2021. This work was supported in part by the National Natural Science Foundation of China under Grant 91638201, Grant 61922013, and Grant 62001023, and in part by the China Postdoctoral Science Foundation under Grant 2020M670163. (Corresponding author: Mengmeng Zhang.)

Dandan Cao and Qiong Ran are with the College of Information Science and Technology, Beijing University of Chemical Technology, Beijing 100029, China (e-mail: 2018200727@buct.edu.cn; ranqiong@mail.buct.edu.cn).

Mengmeng Zhang and Wei Li are with the School of Information and Electronics, Beijing Institute Technology, Beijing 100811, China (e-mail: 7520200002@bit.edu.cn; liwei089@ieee.org).

Digital Object Identifier 10.1109/JSTARS.2021.3072843

As one kind of passive imaging technology, infrared image (IFI), which captures infrared rays radiated inside the object, forms different intensity radiation according to target and background surface temperature, and improves target identification performance. However, the information contained in IFI is relatively simple and not sufficient for complex classification of features. Accordingly, collaborative utilization of the intensity radiation of IFI and the spectral knowledge of HSI holds a clear potential on improving land-cover classification accuracy. However, challenges remained for this collaborative utilization. The information contained in HSI and IFI is different and complementary; therefore, how to integrate the advantages of the multisource heterogeneous properties becomes the key point.

The necessary premise of multisource RS data collaborative utilization is to extract appropriate feature. For hyperspectral data, the spectral variability problem gets hard to handle when background scene is of great complexity. In [15], an enhanced linear mixed model is proposed, which can effectively solve the spectral variability, promotes spectral decomposition, and accurately estimates the abundance map. In addition to spectral information, hyperspectral spatial information is also worth using. As a method of extracting spatial information, mathematical morphology (MM) [16], [17] is a nonlinear, irreversible image analysis method based on the theory of integral geometry, set operations, and geometric probability. The analysis and processing of RS images based on MM has become a major research direction in the field of image processing [18], [19]. In [20] and [21], it was first proposed to introduce morphological algorithms into the detection of small infrared targets, in which the Max-tree and Min-tree were combined to extract targets with large brightness changes, and this method proves the positive effect of morphological algorithms in infrared small targets. For different RS data, it is necessary to select appropriate MM algorithms for achieving better recognition performance. Morphology profile (MP) contains multiple morphological features, which is realized by a series of morphological opening/closing operations with a family of structure elements (SEs) with increasing class sizes. Opening and closing are two common operations in morphology. The opening operation is first to erode and then to dilate the image, aiming at isolating bright structures. The closing operation is first to dilate and then erode the image for suppressing dark structures [22], [23]. On the basis of MP, for multispectral and HSIs, some scholars have proposed extended MP (EMP). That is, through dimension reduction, the MP features for each single band are extracted and, then, integrated for obtaining EMP [24]. However, due to the dependence on SE, the main limitation of MP is that it is difficult to model and extract geometric features with different scale. Therefore, attribute profile (AP) based on morphological attribute filter was proposed. AP can characterize images according to different features represented by attributes [25]. AP is constructed through the component tree (Max/Min-tree). The principle of AP is to calculate the attribute value for each node in the component tree and, then, determine whether the value is greater than the set threshold. The node that is not satisfied with the condition will be removed, and then, the filtered component tree is reconstructed to obtain the features extracted by AP [26], [27]. Similarly, for HSI, extended AP

(EAP) has also been proposed. Moreover, extinction profile (EP) is also constructed based on the component tree. But compared with AP, EP is fully automatic, and the filtering parameters can only be adjusted according to the number of extreme values [28], [29]. Hence, although EP is a more effective algorithm, it is still sensitive to external factors. To deal with these problems, in [30], a morphology algorithm based on topology tree was proposed, which is named local contain profile (LCP). The construction of LCP includes three steps: 1) tree building, 2) filtering, and 3) reconstruction. LCP is more stable than EP, and the dimension of the features extracted by LCP is half of EP. However, for some complex scenarios, due to the filtering strategy of LCP, some effective information will still be lost.

In this article, we propose a threshold-based LCP (TLCP) scheme for more accurate spatial information extraction, and construct a collaborative classification framework for HSI and IFI. First, TLCP is used to extract the spatial information in HSI and IFI. Then, different features are effectively fused for classification. Main contributions can be summarized as follows: 1) By utilizing the differences and complementarities between different source data, an HSI and IFI collaborative classification framework is proposed to improve the classification performance of HSI, and 2) by using TLCP to extract features of HSI and IFI, spatial information of different sources is effectively used. Compared with EP, TLCP is not sensitive to the external factors. And compared with LCP, TLCP can retain more useful information. So, TLCP is more stable and effective than EP and LCP, and the dimension of extracted features is half of EP, which reduces the information redundancy and computational complexity.

The rest of this article is organized as follows. Section II introduces the relative morphological methods that include EP and LCP. Section III introduces TLCP and the HSI and IFI collaborative classification framework. Section IV provides the experimental part and Section V provides some conclusion remarks.

II. RELATED METHODS

In this part, the traditional MM methods including EP and LCP will be introduced.

Recently, some MM methods have been applied for RS data processing. The most commonly used methods for extracting morphological features are EP and LCP. EP can effectively extract spatial information in RS data such as HSI. But EP is built on Max-tree/Min-tree, and Max/Min-tree is based on pixel values between connected domains within the image, which makes the component tree vulnerable to external factors. For example, when there are clouds or shadows, the pixel value of the same position in the image will change, which will change the component tree based on pixel value and affect the feature extraction process. Compared with EP, LCP is a new MM method, which is built based on the topology tree, and the topology tree is constructed according to the inclusion relationship between connected domains, and the inclusion relationship will not change as uncontrollable external factors. Hence, LCP

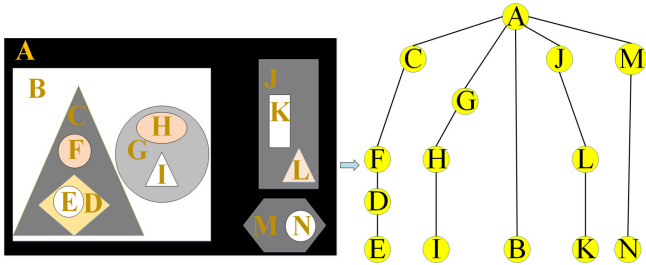


Fig. 1. Construction process of the component tree.

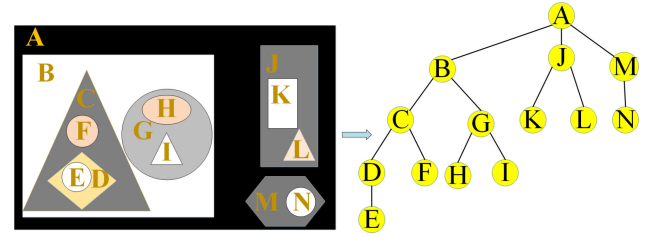


Fig. 3. Construction principle of the topology tree.

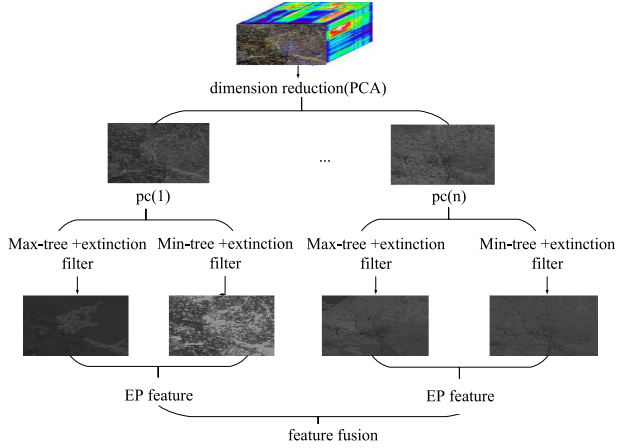


Fig. 2. Flowchart of feature extraction and integration based on EP.

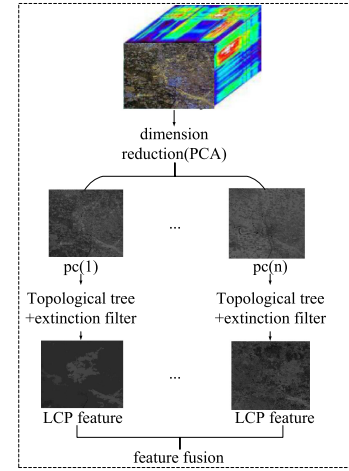


Fig. 4. Flowchart of feature extraction and integration based on LCP.

is more stable. But the process of filtering in LCP could cause loss of useful information.

A. Construction Principle of EP

EP is a representative morphological algorithm built on component trees (Max/Min-tree). In Max-tree, the root node represents the connected region with the smallest pixel value in the whole image, and the leaf node represents the connected domain with the largest local pixel value. The relationship between the root node and the leaf node embodies the hierarchical relationship between connected domains in local regions. The construction process of Max-tree is shown in Fig. 1. A is the root node and represents the connected region with the smallest pixel value, and in this connected area, all pixel value is the same. E, I, B, K, and N are leaf nodes and represent connected areas with the largest local pixel value. By filtering the component tree using extinction filter (EF), features (space, structure, texture, etc.) can be well extracted. EP can adaptively extract the salient features in the image, which can effectively balance global and local attributes representation. However, EP is sensitive to external factors (shadow occlusion and noise); this is because the external environment will affect the pixel value and change the shape of component tree. Fig. 2 shows the process of feature extraction and integration based on EP. As shown in Fig. 2, the feature extraction of EP needs to construct a Max-tree and a Min-tree for each subcomponent derived from PCA operator. Then, all features are merged and used for final

classification. However, this kind of processing is likely to cause the Hughes phenomenon.

B. Construction Principle of Traditional LCP

Compared with EP, LCP is built on topology tree, which extract spatial information contained in HSI in a stable and accurate way. The differences between topology tree and component tree are shown in Figs. 1 and 3. In Fig. 3, A represents the largest connected area that contains all pixels in the whole image. A is the root node. B, J, and M are the second largest connected domains. Particularly, B, J, and M are also the child nodes of A. B contains C and G, so C and G are child nodes of B, and so on. In this way, the topology tree can be constructed. The construction process of LCP is divided into three steps, including the 1) construction of topology tree; 2) extinction filtering; and 3) image reconstruction. The first and third steps will be described in detail ahead. The principle of the EF is to retain the branch of the leaf node that satisfies the condition by the presetting extinction values, and the branch that does not satisfy the leaf node constrained condition would be deleted. The EF of EP is the same as LCP. Fig. 4 shows the process of feature extraction and integration based on LCP. Compared with EP features, LCP features only need to construct a topology tree for each subcomponent, so the dimension of LCP features is half of the dimension of EP features.

The extinction value in the topology tree is defined as follows: Assuming that M is the local minimum connected region in image X , and $\Psi = (\varphi_\lambda)_\lambda$ is a series of decreasing connected

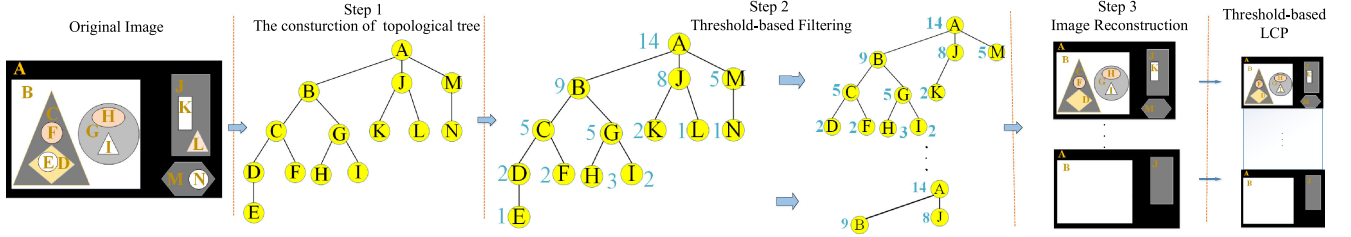


Fig. 5. Flowchart of TLCP construction.

inverse spread transforms. $\epsilon_{\varphi}(M)$ represents the corresponding extinction value associated with Ψ . If it is the global maximum λ value after extinction filtering, M is still the minimum connected region of $\varphi_{\mu}(X)$. The definition of extinction value can be given by the following formula:

$$\varphi_{\mu}(M) = \sup \{ \lambda \geq 0 \mid \forall \mu \leq \lambda, M \subset \text{Min}(\varphi_{\mu}(X)) \} \quad (1)$$

where $\text{Min}(\varphi_{\mu}(X))$ is a set containing all the minimum connected regions of $\varphi_{\mu}(X)$.

EF is a connected filter whose principle is to delete or retain the connected area corresponding to the leaf node and its branch nodes. EF can be defined as follows: Let $\text{Max}(X) = \{M_1, M_2, \dots, M_N\}$ be the set of minimum connected regions in the image X , and each $M_i (i = 1, 2, \dots, N)$ has an extinction value ω_i [defined by (1)]. First, M_i is sorted in a decreasing order according to ω_i ; then, according to threshold n , the first n M_i are selected, and the corresponding leaf nodes are marked; finally, the branches with marked leaf nodes are retained according to the filtering strategy, whereas the branches with unmarked leaf nodes are cut off. This filtering process can be defined as

$$\text{EF}^n = R_g^{\delta}(X) \quad (2)$$

where g is a function of selecting markers. EF obtains $R_g^{\delta}(X)$ through reconstruction operation. g can be expressed as

$$g = \text{Max}_{i=1}^n (M_i^*) \quad (3)$$

where Max is the operation of selecting the minimum connected area with the largest extinction value, M_1^* is the smallest connected area corresponding to the highest extinction value. M_2^* is the minimum connected area corresponding to the second largest extinction value, and so on.

The function of EF is to selectively delete some unimportant areas and retain important areas through artificial control. So, for better effect of features extracting and elimination of noise areas, it is necessary to choose appropriate attributes and set proper extinction values. The threshold setting principle is $\{a^m\}$, ($a = 1, 2, 3, \dots, m = 0, 2, 3, \dots, s - 1$), where a is the basic parameter and s is the number of thresholds.

III. PROPOSED TLCP AND COLLABORATIVE CLASSIFICATION FRAMEWORK

This part consists of the principle of TLCP algorithm, some useful attributes, and collaborative classification framework in detail.

A. Calculation Principle of TLCP

In view of the shortcomings of LCP and EP, this article proposes a new method, named TLCP. TLCP can not only solve the defect problems involved in EP and LCP algorithms, but also achieves better feature extraction and classification performance. TLCP is also constructed based on the topology tree. The construction process of TLCP mainly includes three parts: 1) construction of topology tree; 2) threshold filtering; and 3) image reconstruction. The specific process is shown in Fig. 5.

1) *Construction of Topology Tree*: The topology tree is constructed according to domain relationship (inclusion, adjacent, and separation) between connected areas in the image. Each node in the tree represents a connected area in the graph, and each connected region is only a single node (i.e., the root node represents the largest connected area in the global image, and the leaf node represents the smallest connected area in the local image). The hierarchical relationship between the connected areas represented by the topology tree mainly includes the following.

- 1) The connected areas corresponding to the nodes of the same branch have the inclusion or intersection relationship.
- 2) The connected areas of the nodes, which are in the same level, have the separation or adjacent relationship.
- 3) The connected areas corresponding to the nodes that do not belong to the same branch and do not belong to the same parent node have a separation relationship.

The entire topology tree has only one root node (that is, all connected areas are contained in one root region). The topology tree is constructed as shown in the first part in Fig. 5. The topology tree in this article is calculated based on a quasilinear algorithm. The algorithm also uses a joint search process. The method mainly consists of the following three steps.

- 1) Use the Khalimskey grid to interpolate the scale image to obtain an interpolated image.
- 2) Pixels are sorted in a descending order, and the sorting principle is based on the access order of the interpolated image to the connected regions. A hierarchical queue is used to store the pixel information extracted in order [31].
- 3) Relying on a union-find process to calculate the tree in a reverse order.

In the calculation process of the topology tree, the process of Khalimskey grid interpolation and the priority queue is relatively simple, but the sorting steps are more complicated. A more detailed calculation process of the topology tree can be found in [32]. The calculation method can also be adopted for

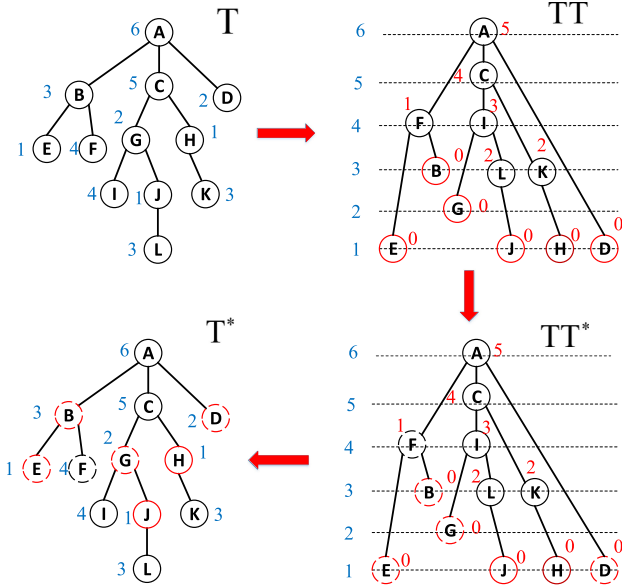


Fig. 6. Construction process and extinction filtering of the second tree. Nodes A–L represent tree nodes, blue values represent the attributes of the first tree, red values represent the attributes of the second tree, and dashed circles indicate the filter nodes when the threshold is set to 2.

constructing the Max/Min-tree, and the only difference is that the sorting steps are different.

2) *Threshold Filtering*: Different from the filtering process in LCP, TLCP uses threshold filtering to improve LCP. Specifically, the topology tree becomes complicated when observed scene is complicated. If each filtering is to remove a *whole branch* that does not satisfy the threshold requirement, it will cause loss of effective information. The key of threshold-based filtering lies in threshold λ and node (connected component) attribute value $\text{attr}(C)$. If $\text{attr}(C) > \lambda$, the node would be retained, otherwise the node would be covered by its parent node. The difference of threshold filtering and extinction filtering is shown in Fig. 8. It can be seen that the former way can retain more information than the latter one. For example, when threshold is set to 2, for the extinction filtering, the branches with nodes containing the first two maximum extinction values are retained, and the other branches are cut, as is shown in Fig. 8(b). But for threshold filtering, only the nodes with attribute value, which are less than 2, need to be discarded, and other nodes and branches are reserved, as shown in Fig. 8(c). The principle of setting the threshold is based on the physical meaning of each attribute. For example, height represents the maximum pixel value minus the minimum pixel value in the connected domain, and the maximum value does not exceed 255. The volume is the maximum pixel value minus the current pixel value and, then, accumulated in connected area. For compactness, circular objects can be retained, and other objects can be cut by setting a threshold value deviating from 1 to perform morphological filtering. For elongation, morphological filtering can be performed by setting a threshold close to 1, which can retain long objects and eliminate other objects.

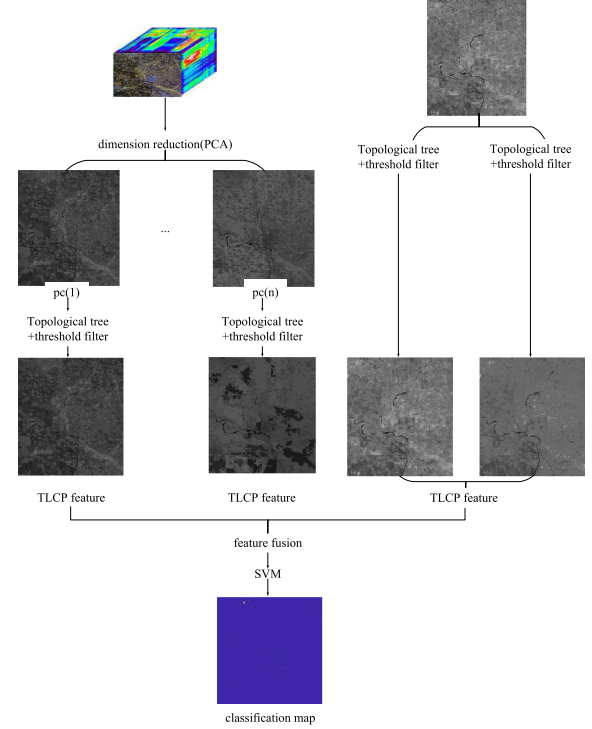


Fig. 7. Collaborative classification framework for multisource hyperspectral data based on TLCP.

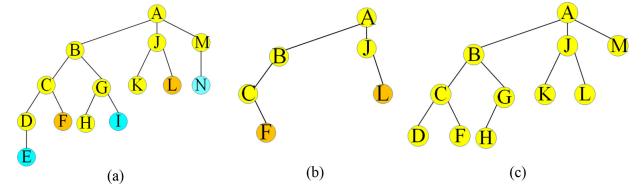


Fig. 8. Difference between LCP and the proposed TLCP. (a) Original topology tree; the orange nodes represent two nodes with the first 2 largest extinction values and the blue nodes represent nodes with attributes values, which is smaller than 2. (b) Result of the extinction filtering. (c) Result of the threshold filtering.

Attributes can be divided into increasing attributes and non-increasing attributes. Increasing attributes include area, height, volume, and bounding box diagonals. Nonincreasing attributes include standard deviation, compactness, elongation, and sharpness [30], [33], [34]. In this article, two increasing attributes (height and volume) and three nonincreasing attributes (standard deviation, compactness, and elongation) are used. For increasing attributes, it is easy for threshold filtering. However, for nonincreasing attributes, the attribute value of leaf node may be larger than the attribute value of the parent node; so, it is difficult to perform filtering operation. In this case, the second tree [35] is necessary to be constructed on the basis of the first tree such that the attribute values corresponding to the tree nodes are in an ordered sequence. The specific construction process is shown in Fig. 6. For increasing attributes, the first tree T and the second tree TT are same. However, for nonincreasing attributes, TT is constructed based on the first tree T [32], and TT can be expressed as the Max/Min-tree. The selection of the Max-tree or Min-tree is mainly determined by the nature

of the attribute function. For example, when filtering undesired shapes, TT selects Min-tree for representation, and the criterion is to make the undesired shapes located near the leaf nodes of TT . On the contrary, if we choose the Max-tree, the desired shape is preserved near the leaf nodes. The connected area of corresponding nodes at the same level in TT share similar shapes. TT^* is the filtered tree on the basis of TT . We calculate which kind of nodes should be cut off based on TT , and all the nodes represented by the dotted circles in Fig. 6 are the points that will be cut. At last, T^* represents the final tree that is pruned based on nonincreasing attribute. More details about the second tree are showed in [35].

3) *Image Reconstruction*: After threshold filtering, the nodes that do not satisfy the threshold requirement are deleted, and relative connected areas are covered by connected areas of a parent node, which leads to the connected areas change in an image. The specific effect is shown in step 3 in Fig. 5. After the filtering operation to topology tree, the tree will be reconstructed into an image, which could be seen as a specific feature obtained by TLCP.

B. Construction of Useful Attributes

There are five attributes used in this article. Among the attributes, height is the contrast attribute, area is the size attribute, volume is the combination of contrast and size attributes, and the bounding box diagonal is a combination of shape and size attributes. These attributes are increasing attributes, which can be calculated by the following formula:

$$\text{Area}(N) = \{\#p \mid p \in N\} \quad (4)$$

$$\text{Height}(N) = \max_{p \in N} f(p) - \min_{p \in N} f(p) \quad (5)$$

$$\text{Volume}(N) = \sum_{p \in N} \left(\max_{p \in N} g(p) - g(p) \right) \quad (6)$$

where N represents a connected area and p indicating a pixel in the connected area. f is a function that obtains the value of a pixel. $g = \pm f$ and the sign is mainly selected according to the direction

$$\text{Std}(N) = \sqrt{\frac{1}{\text{Area}(N)} \sum_{p \in N} (f(p) - K_{\text{gray-level}}(\lambda))^2} \quad (7)$$

where Std is the abbreviation for the standard deviation, $K_{\text{gray-level}}$ is the average intensity of the values of the pixels in the connected region, which can be given as follow:

$$K_{\text{gray-level}}(N) = \frac{1}{\text{Area}(N)} \sum_{p \in N} f(p). \quad (8)$$

The closer the value of compactness is to 1, the connected region is closer to a circle. By setting the threshold of deviation from 1, it is possible to retain the circular object and eliminate other objects, as shown in following equation:

$$\text{Compactness}(N) = \frac{4\pi \text{Area}(N)}{p^2(N)} \quad (9)$$

TABLE I
COMPARISON OF THREE MORPHOLOGICAL METHODS

method	EP	LCP	TLCP
tree	Max/Min-tree	Topology tree	Topology tree
filter	Extinction filter	Extinction filter	Threshold filter
feature dimension		half of EP	half of EP

the more the elongation property deviates from 1, the closer the connected region is to the straight line, and the threshold value close to 1 is set, and the elongated object can be retained and other objects can be eliminated.

$$\text{Elongation}(N) = \frac{l_{\max}(N)}{l_{\min}(N)}. \quad (10)$$

C. HSI and IFI Collaborative Classification Based on Morphological Features

Based on the aforementioned analysis of EP, LCP, and TLCP algorithms, this article proposes a collaborative classification framework for HSI and IFI via TLCP and EP, as shown in Fig. 7. First, TLCP is used for feature extraction of HSI and IFI. Then, features are integrated and fed into SVM, and final classification accuracy and classification map can be obtained. The feature fusion method selected in this article is feature stacking, which is a simple method of data fusion. When extracting the spatial information of the HSI, dimensionality reduction should be executed in advance. The methods of dimensionality reduction include: supervised extraction methods, such as NWFE or band selection [36], [37], as well as unsupervised extraction methods, such as PCA and ICA. PCA is chosen in this article. Let $X_{\text{HSI}_{\text{TLCP}}}$ and $X_{\text{IFI}_{\text{EP}}}$ represent the features of the two data sources obtained by the TLCP and EP, respectively. Fusion feature can be expressed as X

$$X = [X_{\text{HSI}_{\text{TLCP}}}; X_{\text{IFI}_{\text{EP}}}]. \quad (11)$$

D. Comparative Analysis of TLCP, LCP, and EP

Table I lists the similarities and differences of the three methods in terms of tree, filtering method, and feature dimension. Compared with LCP/TLCP, EP is sensitive to the external environment. When the image captured in noises or different lighting conditions, it will have different component trees. It is because when the external environment changes during imaging, the pixel value at the same position will change, and the component tree constructed based on the pixel value will be different. However, for the topology tree, as long as the images are captured at the same time and the same area, the topology tree is the same. In addition, when using EP to extract features, it is necessary to construct a Max-tree and a Min-tree for each subcomponent derived from PCA operator while LCP/TLCP only needs to construct a topology tree for the subcomponents. Therefore, the feature dimension extracted by TLCP/LCP is half of the feature dimension extracted by EP. In general, TLCP/LCP is more stable than EP. Compared with LCP, It can be seen from Fig. 8 that the filtering method of TLCP can better retain effective information, especially for complex

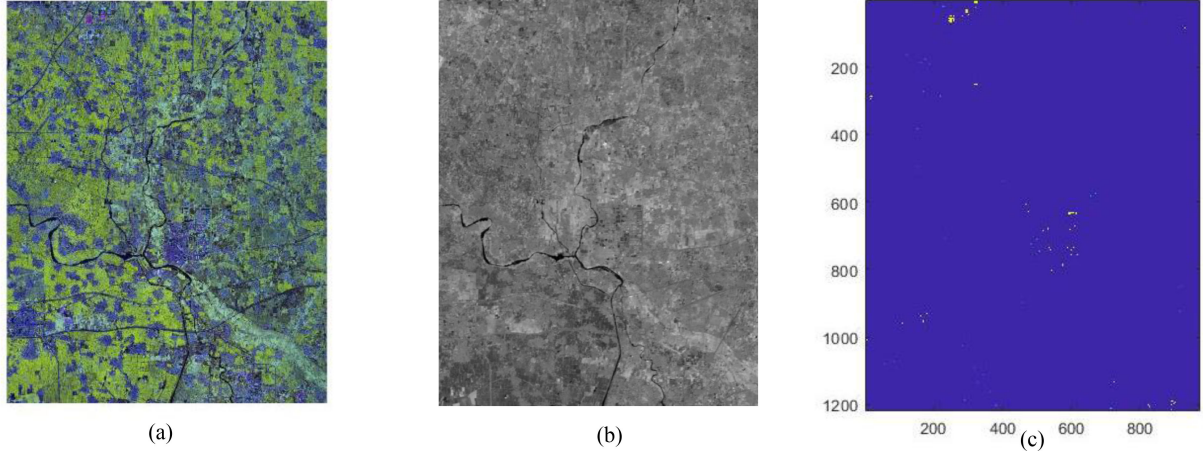


Fig. 9. First kind of GF5 data. (a) HSI. (b) IFI. (c) Groundtruth map.

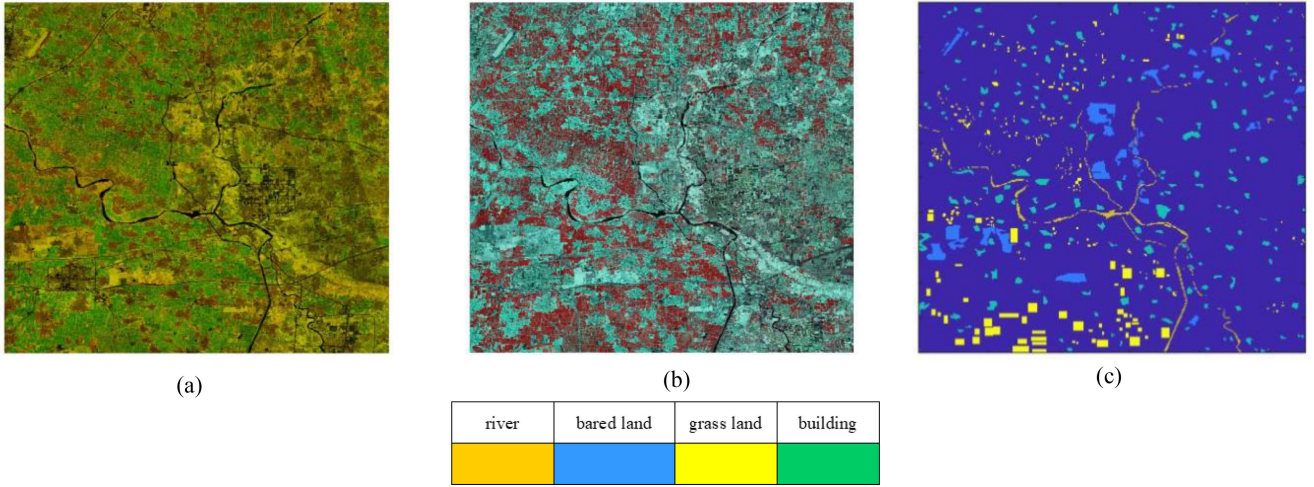


Fig. 10. Second kind of GF5 data. (a) SWIR image. (b) VNIR image. (c) Groundtruth map.

scenes. The following experimental results can also verify the advantages of TLCP over LCP.

IV. EXPERIMENTAL RESULTS AND ANALYSIS

The experiments were carried out based on a real dataset to verify the validity of the proposed collaborative classification framework. Morphological features of five attributes of the data are extracted using TLCP, EP, and LCP, and SVM is utilized as the classifier for obtaining the final classification result.

A. Experimental Data Description

The first dataset used in this article is collected by the GF5 Satellite over Hebei Province in China. This dataset consists of two kinds of RS data, the first data are visible hyperspectral data with the size of $1220 \times 973 \times 150$ and spatial resolution of 30 m. The second data are thermal infrared data with the size of 1220×973 and spatial resolution of 40 m. This dataset contains five types of roof covering named Grayroof normal, Blueroof hot, Redroof normal, Redroof hot, and Blueroof normal. Fig. 9

provides a visual depiction of the HSI, IFI, and groundtruth map in GF5 data.

The second dataset used in this article is collected by the GF5 Satellite over Hebei Province in China. This dataset consists of two kinds of RS data, and the first data are visible near-infrared (VNIR) hyperspectral with the size of $2181 \times 2789 \times 150$ and spatial resolution of 30 m. The second data are shortwave infrared (SWIR) hyperspectral with the size of $2181 \times 2739 \times 180$ and spatial resolution of 30 m. This dataset contains four kinds of sample named river, bared land, grass land and building. Fig. 10 provides a visual depiction of the SWIR, VNIR, and groundtruth map in GF5 data.

B. Experimental Results and Analysis

Overall accuracy (OA), average accuracy (AA), kappa coefficient (Kappa), and other metrics are used here for providing comprehensive investigation and comparisons. During the experiment, five attributes are considered, including two increasing properties (height and volume) and three nonincreasing

TABLE II
NUMBER OF TRAINING AND TEST SAMPLES FOR THE FIRST KIND OF GF5 DATA

No. of class	1	2	3	4	5
name	Grayroof normal	Blueroof hot	Redroof normal	Redroof hot	Blueroof normal
No. of training sample	100	25	100	25	100
No. of test sample	264	30	119	24	730

TABLE III
NUMBER OF TRAINING AND TEST SAMPLES FOR THE SECOND KIND OF GF5 DATA

No. of class	1	2	3	4
name	river	bared land	grass land	building
No. of training sample	100	100	100	100
No. of test sample	9078	23250	23840	33577

TABLE IV
CLASSIFICATION ACCURACY OF THE ORIGINAL IMAGE FOR THE FIRST KIND OF GF5 DATA

No. of class	HSI	IFI	HSI-IFI
1	63.18	64.02	76.89
2	60.00	0	85.33
3	67.11	31.26	53.28
4	24.61	55.00	68.50
5	81.67	70.19	87.95
OA	73.97	64.88	81.32
AA	59.31	44.09	74.39
Kappa	0.5558	0.4062	0.7199

TABLE V
CLASSIFICATION ACCURACY OF THE ORIGINAL IMAGE FOR THE SECOND KIND OF GF5 DATA

No. of class	SWIR	VNIR	SWIR_VNIR
1	90.72	88.22	93.21
2	92.50	95.26	95.24
3	91.19	91.19	90.31
4	99.10	99.10	98.30
OA	93.71	93.71	95.07
AA	93.38	93.44	94.26
Kappa	0.9116	0.9123	0.9307

properties (standard deviation, compactness, and elongation). The number of training and test sample of two datasets are listed in Tables II and III, respectively.

Before giving the experimental results, some notation are defined: h , s , v , c , and e represents height, standard deviation, volume, compactness, and elongation attribute feature extracted by EP/LCP/TLCP, respectively. 5 represents the fusion of five attribute features extracted through EP/LCP/TLCP. The dimension of HSI, SWIR, and VNIR is reduced to 2 using PCA. a and s of extinction filtering are set with 3 and 5. The threshold of TLCP is set as: For the first dataset, $\lambda_c = \{0.3, 0.5, 0.7, 1, 3\}$, $\lambda_e = \{0.05, 0.5, 1, 2.5, 4.5\}$, $\lambda_s = \{1, 5, 25, 55, 85\}$, $\lambda_h = \{1, 5, 10, 30, 70\}$, and $\lambda_v = \{30, 150, 200, 250, 300\}$, for the second dataset, the threshold of c , e , and s are same as the first dataset, but $\lambda_h = \{1, 30, 50, 100, 200\}$ and $\lambda_v = \{30, 150, 200, 350, 500\}$.

Tables IV and V show the classification accuracy based on spectral information of the two datasets, including a single image and multisource image. In addition, it should be noted that the significance of the bold values in Tables IV–XIII are

the maximum value in the corresponding row. Table VI lists the classification performance of HSI in GF5 data using three methods. Table VII shows the classification accuracy of IFI in GF5 data using three methods. Table VIII gives the experimental results of the proposed framework, the comparison methods used in this article are LCP, EP, and fractional Fourier transform (FRFT) [38]. Through comparisons provided in Tables VI–VIII, it can be seen that no matter which method is used, the fusion of data from different data sources can, indeed, improve the classification accuracy. Furthermore, it can also be drawn from Table VI, for HSI, the best accuracy can be obtained by using TLCP, indicating that TLCP is more suitable for extracting spatial information of HSI, and the classification accuracy of each attribute is better than that of LCP and EP. While for IFI in Table VII, the classification performance of LCP and TLCP is better than EP. However, the obtained classification results of TLCP are not optimal; the main reason may be that the threshold value selected for the same scene can retain more useful information for HSI, but for thermal IFI, after filtering, it will cause information redundancy, which makes the results getting worse.

However, although for IFI, TLCP cannot get the best classification results, and for HSI and fusion data, the results of TLCP are the best. It can be seen that in Table VI, the optimal OA, AA, and Kappa of TLCP are 87.08%, 83.69%, and 0.7734, respectively, the optimal OA, AA, and Kappa of LCP are 84.44%, 78.71%, and 0.7311, respectively, and the optimal OA, AA, and Kappa of EP are 84.63%, 72.56%, and 0.7358, respectively. As is shown in Table VIII, the optimal OA, AA, and Kappa of TLCP are 89.00%, 87.77%, and 0.8050, respectively, and the optimal OA, AA, and Kappa of LCP are 85.41%, 71.35%, and 0.7395, respectively. Moreover, the optimal OA, AA, and Kappa of EP are 87.73%, 88.38%, and 0.7902, respectively. It is necessary to pay special attention to the classification effect of the second type of sample in HSI and the fourth type of samples in IFI, for which the classification performance is relatively poor. However, after HSI and IFI are fused, it can be seen from Table VIII that the classification accuracy of the two types of samples has been greatly improved, which also verifies the effectiveness of the proposed fusion classification framework. In addition, it can be seen by comparison that the classification performance of TLCP features is better than that of the original spectral information for the first dataset.

Tables X–XII, respectively, list the classification accuracy of EP, LCP, and TLCP obtained by using a single attribute and multiple attributes in the second GF5 dataset, which are similar to the results of the first GF5 dataset. Whether it is SWIR, VNIR, or the fusion of the two, TLCP can obtain better feature extraction and classification results than EP and LCP. At the same time, through the longitudinal comparison of Tables X–XII, it can be found that when EP is used, for SWIR, the optimal OA, AA, and Kappa are 95.11%, 95.35%, and 0.9316, respectively. For VNIR, the optimal OA, AA, and Kappa are 93.96%, 94.40%, and 0.9174, respectively. For fusion of SWIR and VNIR, optimal OA, AA, and Kappa are 96.78%, 96.88%, and 0.9549, respectively. When LCP is used, for SWIR, the optimal OA, AA, and Kappa are 95.39%, 95.54%, and 0.9354 respectively. For VNIR, the optimal OA/AA and Kappa are

TABLE VI
CLASSIFICATION ACCURACY(%) OF HSI IN GF5 DATA USING EP, LCP, AND TLCP

NO.of class	EP						LCP						TLCP					
	c	e	s	h	v	5	c	e	s	h	v	5	c	e	s	h	v	5
1	61.06	58.33	62.27	80.42	89.92	76.29	66.82	53.41	69.70	73.79	80.26	78.86	64.32	66.21	73.73	82.73	85.15	82.88
2	35.33	56.00	74.66	82.67	74.67	56.00	26.00	37.34	56.00	78.00	82.67	81.33	64.00	56.00	75.34	81.46	86.67	82.00
3	54.79	55.63	69.24	79.66	80.00	66.89	51.42	68.91	68.49	73.44	76.97	76.64	55.96	61.51	65.71	79.83	77.48	74.79
4	5.00	4.17	53.33	33.33	32.61	37.50	0.03	14.62	67.50	25.83	15.00	68.33	35.00	53.26	77.51	84.17	75.00	87.97
5	78.08	79.37	76.90	86.74	85.59	85.88	74.22	61.56	75.89	79.89	84.77	88.38	79.34	83.23	81.42	83.70	86.91	90.82
OA	69.25	70.04	72.27	83.63	84.63	79.67	67.25	66.89	72.70	76.69	81.47	84.44	72.25	75.68	76.81	84.80	85.30	87.08
AA	46.85	50.70	67.28	72.56	72.56	64.51	43.70	47.17	67.52	66.19	67.93	78.71	59.72	64.04	74.74	82.34	82.24	83.69
Kappa	0.4753	0.4895	0.5430	0.7165	0.7358	0.6505	0.4609	0.4552	0.5507	0.6063	0.6828	0.7311	0.5299	0.6370	0.6104	0.7371	0.7481	0.7734

TABLE VII
CLASSIFICATION ACCURACY(%) OF IFI IN GF5 DATA USING EP, LCP, AND TLCP

NO.of class	EP						LCP						TLCP					
	c	e	s	h	v	5	c	e	s	h	v	5	c	e	s	h	v	5
1	61.08	68.49	75.68	75.08	74.09	72.95	66.67	80.76	77.73	78.94	68.41	80.38	54.47	74.24	60.33	70.00	71.39	71.67
2	3.33	3.34	24.00	20.00	15.33	52.67	28.67	1.33	18.67	14.00	7.33	58.67	28.67	0.67	4.67	47.33	25.33	60.00
3	54.79	52.60	56.64	63.70	68.74	70.76	41.68	47.23	61.18	42.52	58.15	66.39	45.38	31.93	32.61	28.07	36.30	61.34
4	60.83	72.50	76.67	79.17	77.50	79.17	33.57	58.33	81.67	75.00	35.83	88.33	42.50	45.83	58.33	56.67	64.16	68.33
5	74.30	58.44	65.94	71.32	69.92	69.56	66.93	63.07	61.92	54.96	66.82	70.99	67.97	68.25	71.26	67.70	70.24	73.07
OA	67.22	58.99	66.34	70.25	69.49	70.21	62.66	63.77	64.71	58.47	64.13	72.68	61.08	63.30	61.20	63.43	63.05	71.12
AA	50.87	51.07	59.79	61.85	61.12	69.02	47.50	50.14	60.23	53.08	47.31	72.95	47.80	44.18	45.44	53.95	53.48	66.88
Kappa	0.4464	0.3694	0.4602	0.5190	0.5105	0.5271	0.3982	0.4181	0.4451	0.3633	0.4321	0.5617	0.3811	0.4107	0.3707	0.4141	0.4046	0.5327

TABLE VIII
CLASSIFICATION ACCURACY(%) OF THE COMBINATION OF HSI AND IFI IN GF5 DATA USING EP, LCP, FRFT, AND TLCP

NO.of class	EP						LCP						FRFT						TLCP					
	c	e	s	h	v	5	c	e	s	h	v	5	0	0.2	0.4	0.6	0.8	1	c	e	s	h	v	5
1	58.79	64.32	74.54	85.53	88.41	78.03	70.00	70.91	75.68	74.09	78.79	74.09	75.00	68.18	69.70	64.77	82.95	75.76	72.95	75.23	78.26	74.39	78.26	80.99
2	84.67	47.33	64.67	90.00	88.67	65.33	54.67	64.00	72.67	87.33	72.67	88.00	66.67	70.00	90.00	93.33	80.00	93.33	74.67	80.67	85.33	92.00	82.67	93.33
3	64.20	61.34	69.25	81.68	87.39	68.40	78.62	64.37	50.25	72.94	50.25	81.68	67.23	70.59	62.18	72.27	52.94	62.18	74.62	61.51	57.65	79.33	57.31	78.17
4	66.67	67.50	74.17	92.50	90.00	71.67	10.00	13.50	10.00	22.50	10.00	20.83	62.50	58.33	87.50	70.83	70.83	70.83	76.67	59.11	73.33	70.83	84.17	92.50
5	83.12	80.74	85.23	87.94	87.43	89.94	82.81	82.02	83.81	87.89	83.81	92.14	83.70	89.59	86.58	85.75	87.26	86.58	89.89	88.96	89.94	89.92	89.86	93.86
OA	75.39	73.94	80.43	86.91	87.73	84.05	77.22	75.82	77.45	81.88	77.45	85.41	78.18	81.66	80.38	82.26	82.26	81.49	83.03	82.18	83.54	85.42	83.62	89.00
AA	71.49	64.25	73.57	87.53	88.38	74.67	59.22	58.96	58.48	68.95	59.10	71.35	71.02	71.34	79.19	74.80	74.80	77.74	77.76	73.10	76.90	81.29	78.45	87.77
Kappa	0.5861	0.5670	0.6633	0.7750	0.7902	0.7205	0.6100	0.6446	0.6064	0.6846	0.6064	0.7395	0.6484	0.6813	0.6673	0.6941	0.6941	0.6815	0.7186	0.6891	0.7114	0.7471	0.7136	0.8050

The order of FRFT in this article is an even order.

TABLE IX
CLASSIFICATION ACCURACY OBTAINED BY FUSING HSI AND IFI FIRST AND THEN EXTRACTING FEATURES

NO.of class	EP						LCP						TLCP					
	c	e	s	h	v	5	c	e	s	h	v	5	c	e	s	h	v	5
1	59.17	55.45	67.42	80.46	82.73	73.33	60.02	62.27	70.46	78.18	77.96	86.14	73.86	69.94	75.47	78.64	79.17	78.26
2	50.67	36.67	60.67	76.67	73.08	57.34	30.00	22.00	44.00	69.33	77.33	80.67	24.67	66.00	76.67	82.67	68.67	94.00
3	64.04	63.70	66.56	52.81	77.11	72.77	58.99	60.17	69.58	75.29	84.87	83.19	68.07	65.38	52.44	73.78	49.92	84.35
4	9.17	20.83	56.67	45.00	39.83	49.17	1.67	5.00	31.66	29.17	15.83	70.83	20.00	20.00	9.17	25.00	11.67	36.67
5	81.40	76.58	79.95	85.07	86.49	84.19	77.20	74.28	77.45	82.77	86.23	87.70	84.63	84.63	83.84	88.79	84.68	87.43
OA	70.90	68.32	72.75	82.66	83.21	79.16	68.69	67.31	73.27	79.52	82.62	86.36	77.63	76.00	77.02	83.55	77.96	83.96
AA	52.89	50.65	66.25	68.00	71.85	67.36	45.58	44.74	58.63	66.95	68.44	81.71	54.25	61.19	59.52	69.78	58.82	76.14
Kappa	0.5052	0.4674	0.5728	0.7207	0.7114	0.6436	0.4692	0.4599	0.5497	0.6492	0.6958	0.7650	0.6145	0.6145	0.5988	0.7103	0.6117	0.7231

TABLE X
CLASSIFICATION ACCURACY(%) OF SWIR IN SECOND DATASET USING EP, LCP, AND TLCP

NO.of class	EP						LCP						TLCP					
	c	e	s	h	v	5	c	e	s	h	v	5	c	e	s	h	v	5
1	86.96	86.40	91.95	92.55	94.42	92.64	79.10	77.67	79.29	93.03	93.50	95.76	89.01	93.04	93.51	94.68	91.65	91.45
2	85.37	82.52	89.86	93.36	91.87	91.69	75.69	73.45	77.81	93.05	91.93	92.41	69.55	94.02	96.09	93.29	96.68	89.42
3	91.20	93.44	94.19	96.07	94.45	96.14	92.80	88.88	91.13	94.00	92.80	94.66	74.07	90.99	91.14	94.08	92.38	93.48
4	96.95	91.45	99.26	99.43	99.11	97.68	90.71	89.71	92.73	98.95	99.35	99.34	97.72	98.32	99.01	99.24	97.08	98.95
OA	89.43	87.02	93.39	95.11	94.76	94.02	82.37	80.52	83.59	94.76	94.45	95.39	84.52	94.13	95.22	95.35	95.62	93.80
AA	90.12	88.45	93.82	95.35	94.96	94.54	84.58	82.43	85.24	94.76	94.40	95.54	82.59	94.09	94.94	95.32	94.45	93.32
Kappa	0.8538	0.8193	0.9076	0.9316	0.9267	0.9166	0.7552	0.7300	0.7718	0.9267	0.9224	0.9354	0.7906	0.9283	0.9327	0.9350	0.9384	0.9137

TABLE XI
CLASSIFICATION ACCURACY(%) OF VNIR IN SECOND DATASET USING EP, LCP, AND TLCP

NO.of class	EP						LCP						TLCP					
	c	e	s	h	v	5	c	e	s	h	v	5	c	e	s	h	v	5
1	84.08	73.38	87.72	90.13	93.37	92.01	54.78	69.76	68.57	93.25	90.28	90.18	92.09	89.26	90.26	93.78	90.51	94.45
2	79.89	73.94	84.20	88.50	87.99	91.37	71.73	67.39	70.80	85.46	87.61	88.39	89.48	92.96	95.79	88.70	93.87	90.83
3	93.20	91.24	93.70	94.68	95.82	95.46	89.31	88.07	88.70	92.88	93.47	95.45	92.20	89.24	88.88	92.40	90.97	94.53
4	96.61	92.46	98.30	98.84	98.95	98.74	93.11	88.71	88.17	98.80	99.44	96.81	98.71	96.76	98.09	99.45	98.07	98.79
OA	86.86	80.55	88.91	92.36	93.15	93.96	78.45	75.89	76.77	91.85	92.12	91.86	92.95	92.68	94.32	93.31	93.87	94.31
AA	88.45	82.76	90.98	93.04	94.03	94.40	77.23	78.48	79.06	92.60	92.70	92.71	93.12	92.06	93.26	93.58	93.35	94.65
Kappa	0.9174	0.7293	0.8592	0.8934	0.9046	0.9155	0.7005	0.6681	0.6774	0.8902	0.8902	0.8866	0.9014	0.8973	0.9189	0.9070	0.9139	0.9206

TABLE XII
CLASSIFICATION ACCURACY(%) OF THE COMBINATION OF SWIR AND VNIR IN GF5 DATA USING EP, LCP, FRFT, AND TLCP

NO.of class	EP						LCP						FRFT						TLCP					
	c	e	s	h	v	5	c	e	s	h	v	5	0	0.2	0.4	0.6	0.8	1	c	e	s	h	v	5
1	90.77	87.56	94.00	95.08	97.48	83.40	82.20	80.94	83.38	95.36	95.20	93.04	93.70	94.40	94.48	95.77	91.83	93.20	94.08	93.02	94.25	96.00	91.41	96.85
2	91.45	85.02	94.02	95.44	94.80	88.49	83.23	80.20	84.05	91.15	90.80	92.81	97.44	96.44	95.41	93.47	97.44	95.27	93.18	93.10	96.12	94.35	92.63	96.50
3	93.77	95.54	95.42	95.98	96.23	97.69	94.18	92.27	92.68	94.30	95.64	95.92	91.79	90.77	92.38	93.06	90.30	91.47	92.77	92.63	92.12	94.52	93.83	93.88
4	97.48	96.53	99.30	98.96	99.00	93.98	96.94	96.43	95.71	99.69	99.28	98.21	97.47	94.28	92.59	98.08	98.95	98.01	98.87	98.51	97.42	99.08	97.23	99.08
OA	93.16	89.87	95.61	96.36	96.78	89.60	87.87	85.97	87.93	94.88	94.73	94.89	95.93	94.98	94.10	95.28	94.70	95.11	94.93	94.51	95.60	96.10	93.69	97.04
AA	93.37	91.16	95.69	96.36	96.88	90.89	89.14	87.46	88.96	95.13	95.23	95.00	95.10	94.47	93.72	95.10	94.63	94.49	94.73	94.32	94.98	95.99	93.78	96.58
Kappa	0.9041	0.8586	0.9385	0.9490	0.9549	0.8573	0.8301	0.8060	0.8315	0.9287	0.9267	0.9286	0.9427	0.9263	0.9172	0.9338	0.9394	0.9313	0.9291	0.9232	0.9382	0.9509	0.9122	0.9385

The order of FRFT in this article is an even order.

TABLE XIII
CLASSIFICATION ACCURACY OBTAINED BY FUSING SWIR AND VNIR FIRST AND THEN EXTRACTING FEATURES

NO.of class	EP						LCP						TLCP					
	c	e	s	h	v	5	c	e	s	h	v	5	c	e	s	h	v	5
1	84.98	90.02	92.42	93.90	95.53	92.61	76.53	74.75	78.65	94.74	94.60	91.81	81.12	90.48	93.13	95.78	94.25	95.78
2	83.59	83.04	91.23	89.32	92.02	93.64	74.49	74.51	81.05	89.91	87.03	93.34	87.03	95.78	96.83	91.93	94.97	92.71
3	92.22	93.11	93.20	96.28	95.81	96.27	92.86	89.70	93.00	95.70	95.25	95.91	92.39	92.37	92.36	94.36	92.96	94.96
4	93.79	92.34	99.13	99.53	99.42	98.31	93.28	89.97	93.71	99.37	99.17	98.67	93.54	98.48	98.67	99.44	98.88	99.34
OA	87.60	87.38	93.90	93.99	95.32	94.52	81.36	80.32	85.16	94.31	93.11	94.66	87.83	94.82	95.94	95.21	95.19	95.54
AA	88.65	89.63	94.00	94.76	95.70	95.21	84.29	82.23	86.60	94.93	94.01	94.93	88.52	94.28	95.25	95.38	95.27	95.70
Kappa	0.8274	0.8241	0.9146	0.9161	0.9346	0.9290	0.7478	0.7274	0.7938	0.9209	0.9046	0.9255	0.8309	0.9272	0.9429	0.9333	0.9326	0.9377

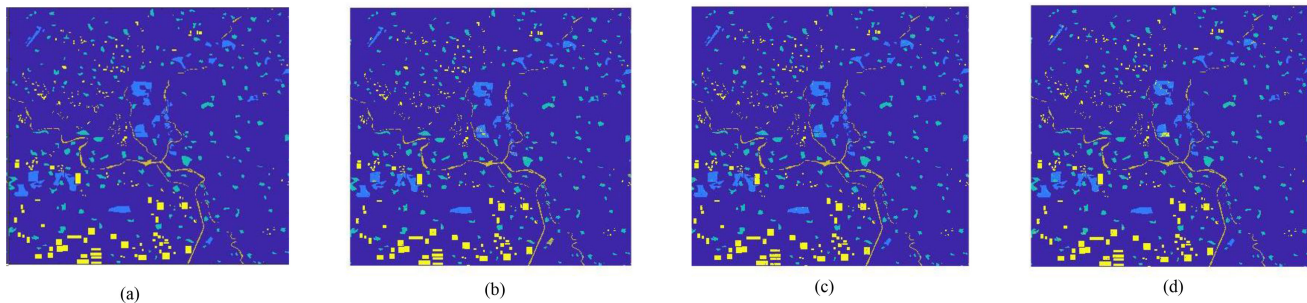


Fig. 11. Groundtruth map and classification map of SWIR by using three methods. (a) Groundtruth map. (b) EP. (c) LCP. (d) TLCP.

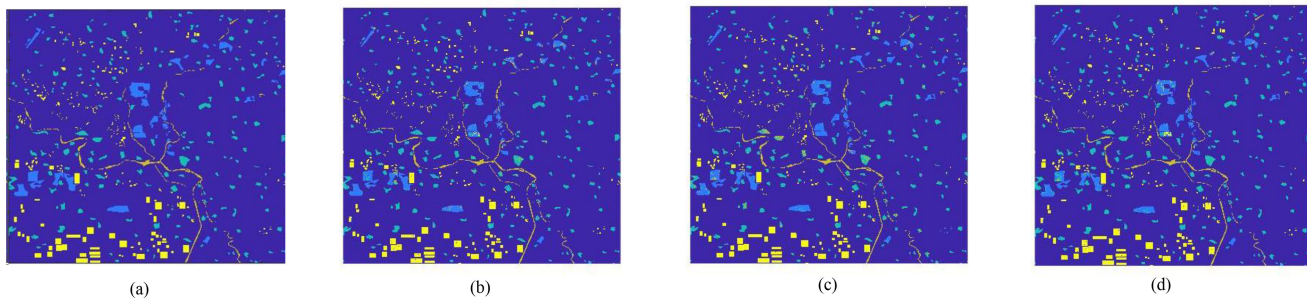


Fig. 12. Groundtruth map and classification map of VNIR by using three methods. (a) Groundtruth map. (b) EP. (c) LCP. (d) TLCP.

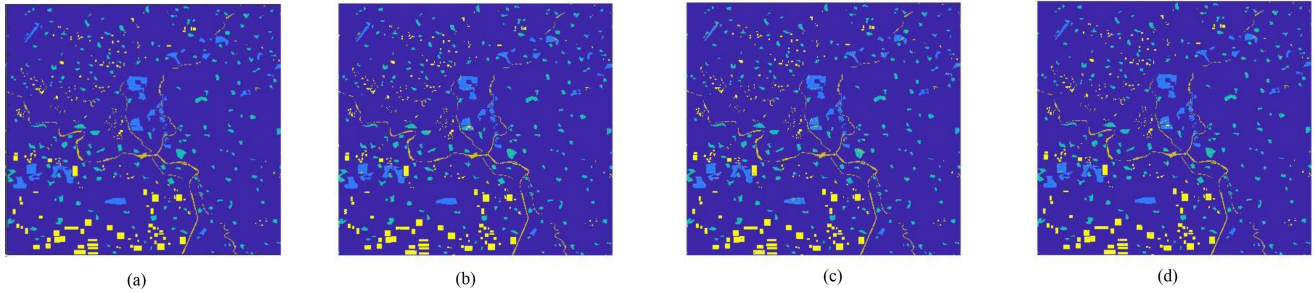


Fig. 13. Groundtruth map and classification map of the fusion of SWIR and VNIR by using three methods. (a) Groundtruth map. (b) EP. (c) LCP. (d) TLCP.

92.12%, 92.71%, and 0.8902, respectively. For fusion of SWIR and VNIR, optimal OA/AA and Kappa are 94.89%, 95.23%, and 0.9287, respectively. When TLCP is used, for SWIR, the optimal OA/AA and Kappa are 95.62%, 95.32%, and 0.9384, respectively. For VNIR, the optimal OA/AA and Kappa are 94.32%, 94.65%, and 0.9206, respectively. For fusion of SWIR and VNIR, optimal OA/AA and Kappa are 97.04%, 96.58%, and 0.9385, respectively. It can be seen from these data that after integrating TLCP features, the classification performance has been improved, and the same effect can be obtained for EP features, but for LCP, after the fusion, the classification accuracy has decreased. This may be because the LCP features of these two kinds of data do not have good complementarity and difference. After fusion, it will cause dimensional explosion and affect classification performance. In addition, it can be seen by comparison that the classification performance of TLCP features is better than that of the original spectral information for the second dataset, too. In addition, the results of FRFT can be seen in Table XII.

The proposed method is to first extract the features of the image and then classify the features after fusion. In order to verify the effectiveness of the method, we also did experiments of first fusing the data and then extracting the features, and then performing the classification. The experimental results are shown in Tables IX and XIII. Comparing Table IX with Tables VIII, XIII, and XII, it can be found that extracting features first and then fusing the features can obtain a better classification effect than fusing the images first and then performing feature extraction. This may be because the information obtained by first fusing the images, then reducing the dimensionality of the fused images and then performing feature extraction will be lost, which is not conducive to classification.

In order to more intuitively show the feature extraction and classification effects of various mathematical morphological algorithms (EP, LCP, and TLCP) on the second GF5 dataset, this article gives a classification effect diagram of each method, as shown in Figs. 11–13, which are consistent with the results shown in Tables X–XII.

V. CONCLUSION

In this article, an HSI and IFI collaborative framework based on TLCP was proposed. Complementary data were fused by the

proposed framework for classification. And five morphological attributes were used for feature extraction. In this article, the proposed framework was applied on two real datasets. It can be proved that extracting features from the image first and then performing feature-level fusion can improve classification performance. Finally, it can be concluded that the classification performance of HSI can be improved by the fusion of data from different sources, concluded that the accuracy of multiattribute features was better than that of single attribute.

REFERENCES

- [1] Y. Huang, C. Zhong-Xin, Y. Tao, H. Xiang-Zhi, and G. Xing-Fa, "Agricultural remote sensing big data: Management and applications," *J. Integrative Agriculture*, vol. 17, no. 9, pp. 1915–1931, 2018.
- [2] D. Hong *et al.*, "More diverse means better: Multimodal deep learning meets remote sensing imagery classification," *IEEE Trans. Geosci. Remote Sens.*, vol. 59, no. 5, pp. 4340–4354, May 2021.
- [3] D. Hong, L. Gao, J. Yao, B. Zhang, P. Antonio, and J. Chanussot, "Graph convolutional networks for hyperspectral image classification," *IEEE Trans. Geosci. Remote Sens.*, to be published, 2020.
- [4] F. Li, R. Feng, W. Han, and L. Wang, "An augmentation attention mechanism for high-spatial-resolution remote sensing image scene classification," *IEEE J. Sel. Topics Appl. Earth Observ. Remote Sens.*, vol. 13, pp. 3862–3878, 2020.
- [5] L. Zhang, Z. Chen, L. Zheng, and Q. Tong, "The application of hyperspectral remote sensing to coast environment investigation," *Acta Oceanologica Sin.*, vol. 28, no. 2, pp. 1–13, 2009.
- [6] H. Yu, L. Gao, W. Liao, B. Zhang, A. Pižurica, and W. Philips, "Multiscale superpixel-level subspace-based support vector machines for hyperspectral image classification," *IEEE Geosci. Remote Sens. Lett.*, vol. 14, no. 11, pp. 2142–2146, Nov. 2017.
- [7] Q. Shi, X. Tang, T. Yang, R. Liu, and L. Zhang, "Hyperspectral image denoising using a 3-D attention denoising network," *IEEE Trans. Geosci. Remote Sens.*, to be published, doi: [10.1109/TGRS.2020.3045273](https://doi.org/10.1109/TGRS.2020.3045273).
- [8] Q. Shi *et al.*, "Domain adaption for fine-grained urban village extraction from satellite images," *IEEE Geosci. Remote Sens. Lett.*, vol. 17, no. 8, pp. 1430–1434, Aug. 2020.
- [9] J. Ren, J. Zabalza, S. Marshall, and J. Zheng, "Effective feature extraction and data reduction in remote sensing using hyperspectral imaging [applications corner]," *IEEE Signal Process. Mag.*, vol. 31, no. 4, pp. 149–154, Jul. 2014.
- [10] Q. Du, L. Zhang, B. Zhang, X. Tong, P. Du, and J. Chanussot, "Foreword to the special issue on hyperspectral remote sensing: theory, methods, and applications," *IEEE J. Sel. Topics Appl. Earth Observ. Remote Sens.*, vol. 6, no. 2, pp. 459–465, Apr. 2013.
- [11] Q. Cao, Y. Zhong, A. Ma, and L. Zhang, "Urban land use/land cover classification based on feature fusion fusing hyperspectral image and Lidar data," in *Proc. IEEE Int. Geosci. Remote Sens. Symp.*, 2018, pp. 8869–8872.
- [12] X. Zhao *et al.*, "Joint classification of hyperspectral and Lidar data using hierarchical random walk and deep CNN architecture," *IEEE Trans. Geosci. Remote Sens.*, vol. 58, no. 10, pp. 7355–7370, Oct. 2020.

- [13] J. Hu, P. Ghamisi, A. Schmitt, and X. X. Zhu, "Object based fusion of polarimetric SAR and hyperspectral imaging for land use classification," *Proc. 8th Workshop Hyperspectral Image Signal Process., Evol. Remote Sens.*, 2016, pp. 1–5.
- [14] P. R. Marpu and S. S. Martinez, "Object-based fusion of hyperspectral and Lidar data for classification of urban areas," *Proc. 7th Workshop Hyperspectral Image Signal Process., Evol. Remote Sens.*, 2015, pp. 1–4.
- [15] D. Hong, N. Yokoya, J. Chanussot, and X. X. Zhu, "An augmented linear mixing model to address spectral variability for hyperspectral unmixing," *IEEE Trans. Image Process.*, vol. 28, no. 4, pp. 1923–1938, Apr. 2019.
- [16] H. H. Jam, *Morphological Image Operators*. Boston, MA, USA: Academic, 1994.
- [17] L. Hu, C. Qi, and Q. Wang, "Spectral-spatial hyperspectral image classification based on mathematical morphology post-processing," *Procedia Comput. Sci.*, vol. 129, pp. 93–97, 2018.
- [18] M. Jiang and G. Chen, "Research and application of metallographical image edge detection based on mathematical morphology," *Proc. 3rd Int. Symp. Intell. Inf. Technol. Appl.*, vol. 3, 2009, pp. 477–480.
- [19] J. Zhang, S. Mavromatis, Q. Meng, J. Sequeira, Y. Sun, and Y. Zhang, "Using mathematical morphology on Lidar data to extract information from urban vegetation," in *Proc. IEEE Int. Geosci. Remote Sens. Symp. Sens.*, 2016, pp. 1281–1283.
- [20] M. Zhao, L. Li, W. Li, R. Tao, L. Li, and W. Zhang, "Infrared small-target detection based on multiple morphological profiles," *IEEE Trans. Geosci. Remote Sens.*, to be published, doi: [10.1109/TGRS.2020.3022863](https://doi.org/10.1109/TGRS.2020.3022863).
- [21] M. Zhao, W. Li, L. Li, P. Ma, Z. Cai, and R. Tao, "Three-order tensor creation and Tucker decomposition for infrared small-target detection," *IEEE Trans. Geosci. Remote Sens.*, to be published, doi: [10.1109/TGRS.2020.3022863](https://doi.org/10.1109/TGRS.2020.3022863).
- [22] F. Safa and G. Flouzat, "Speckle removal on radar imagery based on mathematical morphology," *Signal Process.*, vol. 16, no. 4, pp. 319–333, 1989.
- [23] V. D. Witte, G. Thoonen, P. Scheunders, A. Pizurica, and W. Philips, "Classification of multi-source images using color morphological profiles," in *Proc. IEEE Int. Geosci. Remote Sens. Symp.*, 2011, pp. 3919–3922.
- [24] M. Fauvel, J. Chanussot, and J. A. Benediktsson, "Kernel principal component analysis for the construction of the extended morphological profile," in *Proc. IEEE Int. Geosci. Remote Sens. Symp.*, 2009, pp. II-843–II-846.
- [25] M. Pedernana, P. R. Marpu, M. D. Mura, J. A. Benediktsson, and L. Bruzzone, "Classification of remote sensing optical and Lidar data using extended attribute profiles," *IEEE J. Sel. Topics Signal Process.*, vol. 6, no. 7, pp. 856–865, Nov. 2012.
- [26] G. Cavallaro, N. Falco, M. D. Mura, and J. A. Benediktsson, "Automatic attribute profiles," *IEEE Trans. Image Process.*, vol. 26, no. 4, pp. 1859–1872, Apr. 2017.
- [27] A. Tombak, I. Türkmenli, E. Aptoula, and K. Kayabol, "Pixel-based classification of SAR images using feature attribute profiles," *IEEE Geosci. Remote Sens. Lett.*, vol. 16, no. 4, pp. 564–567, Apr. 2019.
- [28] P. Ghamisi, L. R. R. Souza, J. A. Benediktsson, R. Lotufo, and X. X. Zhu, "Extinction profiles: A novel approach for the analysis of remote sensing data," *Proc. IEEE Int. Geosci. Remote Sens. Symp.*, 2016, pp. 5122–5125.
- [29] P. Ghamisi, R. Souza, J. A. Benediktsson, X. X. Zhu, L. Rittner, and R. Lotufo, "Extended extinction profile for the classification of hyperspectral images," *Proc. 8th Workshop Hyperspectral Image Signal Process., Evol. Remote Sens.*, 2016, pp. 1–4.
- [30] W. Li, Z. Wang, L. Li, and Q. Du, "Feature extraction for hyperspectral images using local contain profile," *IEEE J. Sel. Topics Appl. Earth Observ. Remote Sens.*, vol. 12, no. 12, pp. 5035–5046, Dec. 2019.
- [31] Y. Xu, "Tree-based shapes spaces: Definition and application in image processing and computer vision," Ph.D. dissertation, Université Paris-Est, Champs-sur-Marne, France, 2013.
- [32] T. Géraud, E. Carlinet, S. Crozet, and L. Najman, "A quasi-linear algorithm to compute the tree of shapes of nD images," *Int. Symp. Math. Morphol. Appl. Signal Image Process.*, 2013, pp. 98–110.
- [33] A. G. Silva and R. de Alencar Lotufo, "New extinction values from efficient construction and analysis of extended attribute component tree," *Proc. 21st Brazilian Symp. Comput. Graph. Image Process.*, 2008, pp. 204–211.
- [34] E. J. Breen and R. Jones, "Attribute openings, thinnings, and granulometries," *Comput. Vis. Image Understanding*, vol. 64, no. 3, pp. 377–389, 1996.
- [35] Y. Xu, T. Gaud, and L. Najman, "Morphological filtering in shape spaces: Applications using tree-based image representations," *Proc. 21st Int. Conf. Pattern Recognit.*, 2012, pp. 485–488.
- [36] P. Ghamisi, J. A. Benediktsson, G. Cavallaro, and A. Plaza, "Automatic framework for spectral-spatial classification based on supervised feature extraction and morphological attribute profiles," *IEEE J. Sel. Topics Appl. Earth Observ. Remote Sens.*, vol. 7, no. 6, pp. 2147–2160, Jun. 2014.
- [37] P. Ghamisi, J. A. Benediktsson, and J. R. Sveinsson, "Automatic spectral-spatial classification framework based on attribute profiles and supervised feature extraction," *IEEE Trans. Geosci. Remote Sens.*, vol. 52, no. 9, pp. 5771–5782, Sep. 2014.
- [38] R. Tao, X. Zhao, W. Li, H. Li, and Q. Du, "Hyperspectral anomaly detection by fractional Fourier entropy," *IEEE J. Sel. Topics Appl. Earth Observ. Remote Sens.*, vol. 12, no. 12, pp. 4920–4929, Dec. 2019.